Geophysical Research Letters

RESEARCH LETTER
10.1029/2025GL119186

# Connecting Mixing to Upwelling Along the Ocean's Sloping Boundary

**Alberto C. Naveira Garabato**[1], **Carl P. Spingys**[2], **Bieito Fernández Castro**[1], **Nicole Couto**[3], **Henri F. Drake**[4], **Alexander Forryan**[1], **Zhiyuan Gao**[1,5], **Yuchen Ma**[6], **Herlé Mercier**[7], **Marie-José Messias**[8], **Xiaozhou Ruan**[9], **Gunnar Voet**[3], **Bethan L. Wynne-Cattanach**[3], **Raffaele Ferrari**[6], **and Matthew H. Alford**[3]

[1]Ocean and Earth Science, University of Southampton, Southampton, UK, [2]National Oceanography Centre, Southampton, UK, [3]Scripps Institution of Oceanography, University of California San Diego, La Jollxa, CA, USA, [4]Department of Earth System Science, University of California Irvine, Irvine, CA, USA, [5]Key Laboratory of Physical Oceanography, Ocean University of China, Qingdao, China, [6]Department of Earth, Atmospheric and Planetary Sciences, Massachusetts Institute of Technology, Cambridge, MA, USA, [7]Laboratoire de Physique des Océans, CNRS, UMR 6523 CNRS/Ifremer/IRD/UBO, Ifremer Centre de Brest, Plouzané, France, [8]College of Life and Environmental Sciences, University of Exeter, Exeter, UK, [9]Department of Earth and Environment, Boston University, Boston, MA, USA

**Key Points:**

- The drivers of the rapid along-boundary upwelling observed by the BLT-Recipes dye experiment in a continental-slope canyon are investigated
- It is shown that along-boundary up-welling stems from turbulent mixing cells up to 250 m high, generated by sheared tidal flows
- The turbulence mixes the denser waters in the canyon with neighboring lighter waters, causing the dense waters to upwell along the boundary

**Supporting Information:**

Supporting Information may be found in the online version of this article.

**Correspondence to:**

A. C. Naveira Garabato,
acng@soton.ac.uk

**Citation:**

Naveira Garabato, A. C., Spingys, C. P., Castro, B. F., Couto, N., Drake, H. F., Forryan, A., et al. (2025). Connecting mixing to upwelling along the ocean's sloping boundary. *Geophysical Research Letters*, *52*, e2025GL119186. https://doi.org/10.1029/2025GL119186

Received 7 SEP 2025
Accepted 29 OCT 2025

**Author Contributions:**

**Conceptualization:** Carl P. Spingys, Bieito Fernández Castro, Gunnar Voet, Raffaele Ferrari, Matthew H. Alford
**Formal analysis:** Carl P. Spingys, Bieito Fernández Castro, Zhiyuan Gao, Yuchen Ma, Matthew H. Alford
**Funding acquisition:** Marie-José Messias, Gunnar Voet, Raffaele Ferrari, Matthew H. Alford
**Investigation:** Carl P. Spingys, Bieito Fernández Castro, Nicole Couto, Henri F. Drake, Alexander Forryan, Zhiyuan Gao, Yuchen Ma, Herlé Mercier, Marie-José Messias, Xiaozhou Ruan, Gunnar Voet, Bethan L. Wynne-Cattanach, Raffaele Ferrari, Matthew H. Alford



**Abstract** Deep-ocean upwelling, driven by small-scale turbulence, plays a key role in climate by regulating the ocean's capacity to sequester heat and carbon. Recent theoretical studies have hypothesized that such upwelling may primarily occur within a bottom boundary layer (BBL) along the sloping seafloor. A dye experiment in a continental-slope canyon during the BLT-Recipes program revealed very rapid BBL-focussed upwelling, endorsing this notion. Here, we elucidate the dynamical connection between the mixing and the upwelling. We show that along-canyon upwelling stems from episodic turbulent mixing cells up to 250 m high, generated by tides sweeping up- and down-canyon. The tidal currents support a vertical shear that periodically advects dense waters over slower-flowing lighter waters, reducing BBL stratification. This triggers instabilities that mix the dense waters with neighboring lighter waters, resulting in net along-boundary upwelling. Our findings substantiate the view that deep-ocean upwelling can predominantly occur along the ocean's sloping boundaries.

**Plain Language Summary** Deep-ocean upwelling, driven by centimeter-sized turbulent whirls, plays a key role in climate by regulating the ocean's capacity to sequester heat and carbon. Recent theoretical studies have hypothesized that this upwelling may occur mainly within a thin layer adjacent to the sloping seafloor. A recent dye experiment in a canyon at the edge of a North Atlantic basin supports this hypothesis, by revealing that very rapid upwelling occurs along the canyon's sloping axis. Here, we determine the turbulent processes driving the upwelling. We show that the upwelling results from turbulent mixing events up to 250 m high, which are generated by tidal currents sweeping up and down the canyon. As the speed of these currents typically decreases with depth, the tides cause dense waters originating deep in the canyon to flow over lighter shallower waters. This reduces the vertical gradient of density, priming the canyon for dynamical instabilities and turbulence. When this turbulence mixes dense waters with neighboring lighter waters, the dense waters become lighter and thus upwell along the canyon.

## 1. Introduction

Small-scale turbulent mixing has long been recognized as the key driver of deep-ocean diapycnal upwelling, through which dense abyssal waters of high-latitude origin are transformed into lighter, mid-depth waters (de Lavergne et al., 2016, 2021; Melet et al., 2021; Munk, 1966). Starting with Walter Munk's work in the 1960s, it has been extensively argued that upwelling is broadly distributed across the global ocean below ∼1,000 m (Lumpkin & Speer, 2007; Munk & Wunsch, 1998; Talley, 2013), and that its underpinning mixing is induced principally by the breaking of internal waves radiating from rough topography (Kunze, 2017b; MacKinnon et al., 2017; Munk & Wunsch, 1998). A conundrum in this argument is raised, however, by observations of the deep-ocean internal wavefield and associated turbulence: the intensity of such turbulence above rough topography—where the turbulence is commonly most vigorous—usually increases with depth (Kunze, 2017a; Waterhouse et al., 2014; Whalen et al., 2020). This vertical structure of the turbulence implies that water parcels subject to wave breaking mix more rapidly with underlying denser layers than with overlying lighter waters, and

**Methodology:** Carl P. Spingys, Bieito Fernández Castro, Zhiyuan Gao, Yuchen Ma, Gunnar Voet, Bethan L. Wynne-Cattanach, Raffaele Ferrari, Matthew H. Alford
**Project administration:** Raffaele Ferrari, Matthew H. Alford
**Validation:** Zhiyuan Gao
**Writing – review & editing:** Raffaele Ferrari, Matthew H. Alford

so must become denser and downwell—not upwell—across the ocean's density stratification (de Lavergne et al., 2016; Ferrari et al., 2016).

A potential solution is provided by a body of recent theoretical work (de Lavergne et al., 2016; Drake et al., 2020; Ferrari et al., 2016; Polzin & McDougall, 2021), founded on the principle that mixing must vanish at the ocean's solid boundaries. Since water parcels close to the seabed may only mix with overlying lighter waters, they must become lighter and *upwell* across stratification. If topography is sloped, as is often the case, such lightening of near-boundary waters results in an upward along-boundary flow that transports those waters to shallower depths (Garrett, 1990). Thus, in this alternative view, deep-ocean diapycnal upwelling would expectedly occur via focussed and rapid along-boundary flows within an O (10 m)-thick layer with reduced stratification—the bottom boundary layer (BBL)—directed up sloping topography, with the downward decrease in mixing across the BBL governing the upwelling's intensity. Direct observational evidence in support of this scenario is lacking, however, so that the fundamental physics of BBL mixing and upwelling remain the focus of a vibrant discussion (Armi, 1979a, 1979b; Garrett, 1979; Polzin & McDougall, 2021).

To address this evidence gap, the U.K.-U.S. Bottom Boundary Layer Turbulence and Abyssal Recipes (BLT-Recipes) program performed a suite of measurements of turbulent mixing, diapycnal upwelling and their driving processes along a paradigmatic ocean boundary: a continental-slope canyon, the likes of which occupy over one-fifth of all continental slopes bordering the global ocean (Harris & Whiteway, 2011; Harris et al., 2014). Measurements of the dispersion of a fluorescein dye injected near the seabed (Wynne-Cattanach et al., 2024a) revealed exceptionally rapid diapycnal upwelling of O ($10^{-3}$ m $s^{-1}$) [O (100 m $d^{-1}$), or roughly 10,000 times the global-mean deep-ocean upwelling rate (de Lavergne et al., 2021; Lumpkin & Speer, 2007; Munk, 1966; Munk & Wunsch, 1998; Talley, 2013)] along the canyon's thalweg. Here, we assess the dynamical connection between turbulent mixing within the canyon and the strong along-boundary upwelling.

## 2. Data and Methods

### 2.1. Data

The canyon targeted by BLT-Recipes is approximately 30 km long and 8 km wide at its entry, and is located in the Rockall Trough (Northeast Atlantic; Figure 1a)—a basin characterized by generally moderate deep-ocean stratification and circulation (Holliday et al., 2015) and barotropic tidal currents (Stanev & Ricker, 2020). The observations considered here were obtained in July-October 2021, using both vessel-deployed and moored instrumentation. The ship-based measurements included (Figure 1a): an along-canyon section of 11 full-depth hydrographic and (temperature and shear) microstructure profiles, which captures the general increase in the intensity of turbulence with proximity to the seabed (Figure 1b) characteristic of regions of rough topography (Waterhouse et al., 2014; Kunze, 2017a, 2017b); 6 finely-resolved FastCTD (Klymak et al., 2006) timeseries of hydrographic and temperature microstructure profiles within the canyon spanning at least one semidiurnal tidal cycle (Alford et al., 2025); and the dye dispersion measurements (Wynne-Cattanach et al., 2024a). The dye-derived diapycnal velocity of O ($10^{-3}$ m $s^{-1}$) is equivalent to a warming of ∼0.3°C $d^{-1}$ as water parcels upwell across the canyon's stable background stratification, which is primarily determined by temperature (Figure 1b; see also Supporting Information S1). High- (vertical and temporal) resolution records of turbulent fluctuations in three-dimensional velocity and temperature were acquired by a mooring instrumented with an acoustic Doppler current profiler (ADCP), 8 modular acoustic velocity meters and 83 thermistors, distributed across the deepest 300 m of the water column. The mooring was deployed near the canyon's head (Figure 1a) for 89 days (i.e., ∼172 semidiurnal and ∼106 inertial periods), thereby affording robust statistical sampling of variability in turbulent parameters within the canyon across a broad range of frequencies (including tidal and near-inertial). See Supporting Information S1 for further details.

### 2.2. Calculation of Turbulent Mixing Rates From Mooring-Based Temperature Observations

To assess the evolution of mixing within the canyon, the rate of dissipation of temperature variance, $\chi$, was computed from temperature timeseries acquired with each of the 83 fast-sampling (1 Hz) thermistors in the mooring. $\chi$ is estimated from temperature records by fitting a theoretical model of inertial-subrange turbulence to measured temperature spectra (Bluteau et al., 2013; Shaw et al., 2001; Sreenivasan, 2018). See Supporting Information S1 for a full model description. Implicit in the model are the assumptions of: Taylor's frozen field, used to relate horizontal wavenumber spectra to the measured frequency spectra (Bluteau et al., 2013; Shaw

10.1029/2025GL119186

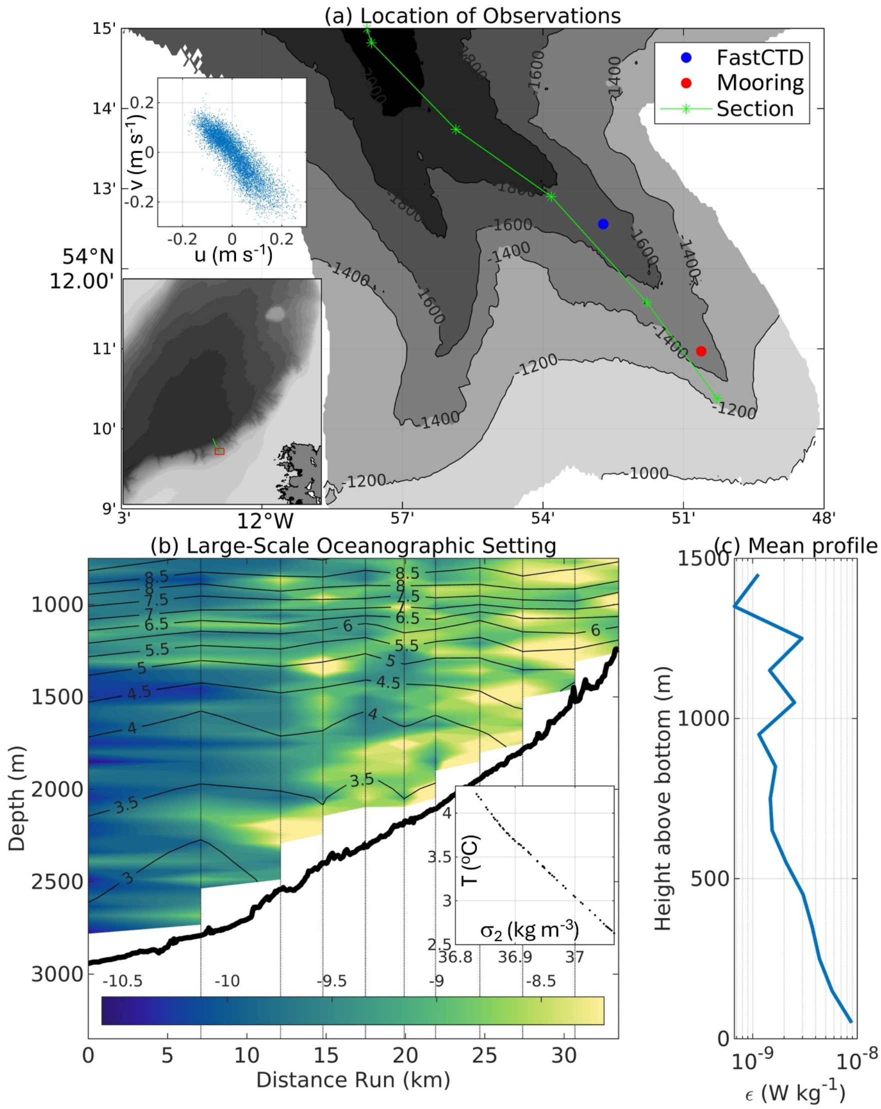


**Figure 1.** Overview of BLT-Recipes experimental domain and observations. (a) Topography of the Rockall Trough in the Northeast Atlantic (lower inset), and of the continental-slope canyon measured during the BLT-Recipes experiment (main panel) with measurement locations indicated by instrument-referencing symbols. The near-bottom (averaged over a height above bottom range of 50–300 m) velocity at the location of the mooring is shown in the upper inset, and indicates that tidal fluctuations in the in-canyon flow are predominantly oriented along the canyon. (b) Logarithm of the rate of turbulent kinetic energy dissipation ($\varepsilon$, shading) and potential temperature (contours) along the canyon's thalweg (section marked in (a)). The inset illustrates the potential temperature ($T$)—density relationship observed within the canyon, where the density variable shown ($\sigma_2$) is the potential density relative to 2,000 dbar. (c) Along-canyon-mean profile of $\varepsilon$ versus height above bottom.

et al., 2001); a constant dissipation ratio, $\Gamma$, which relates the rate of turbulent kinetic energy dissipation, $\varepsilon$, to a buoyancy flux (Gregg et al., 2018); and a sole dependence of buoyancy frequency on temperature, found to accurately hold within the canyon. An estimate of $\chi$ was obtained for each thermistor every 5 min by first computing mean temperature spectra in 5-min segments and, second, fitting the theoretical model for periods of 10–100 s (or a suitably narrower range for near-bottom thermistors) representative of the inertial subrange. $\Gamma$ was taken as 0.2 (as pertinent to much of the ocean; Gregg et al., 2018), but the sensitivity of $\chi$ to this choice was explored by repeating the calculation with $\Gamma = 0.4$ (likely more appropriate to our measured canyon; Alford et al., 2025). The calculation of $\chi$ from thermistor data entails several other practical computation choices, which introduce uncertainty. This uncertainty is discussed in the Supporting Information S1, and found to be typically a factor of <2.

The mooring-based estimates of $\chi$ are of a subtly different nature to those acquired by the microstructure profilers—a distinction that has both advantages and challenges for our work. Profiler-based $\chi$ measurements are obtained at the closing stages of the turbulent cascade of temperature variance, that is, near the dissipative (Kolmogorov) scale at which mixing takes place. Thus, they offer an accurate, relatively assumption-free view of local mixing. In contrast, mooring-based $\chi$ values are derived from observations within the inertial subrange, such that the measured temperature variance is yet to cascade further downscale before reaching the dissipative scale. A simple estimate of the timescale of the downscale cascade ($\langle T'^2\rangle/\chi$, where $\langle T'^2\rangle$ is the characteristic thermistor-measured potential temperature ($T$) variance on inertial-subrange timescales) suggests that it may take several hours for that variance to be dissipated. Consequently, mooring-based $\chi$ values provide an assumption-heavier, but integrated metric of the in-canyon mixing. The integral character of mooring-based $\chi$ estimates is arguably advantageous to our goal of connecting upwelling to mixing rates, as it reduces the sensitivity of the calculation to the precise location of the mooring—which effectively samples mixing conditions along a substantial segment of the canyon. Since the in-canyon flow is highly rectilinear (oriented along-canyon) and varies primarily on semidiurnal tidal timescales, the along-canyon advective lengthscale corresponding to $\langle T'^2\rangle/\chi$ may be estimated as O (100–1,000 m), given a characteristic along-canyon tidal velocity of $\sim$0.1 m s$^{-1}$ (Figure 1a).

A further advantage of mooring measurements is that they are approximately Eulerian, and thereby provide unbiased sampling of all phases of the tidal cycle. Whereas the mooring's uppermost instruments move horizontally by only <50 m during one such cycle, microstructure profilers may drift with the tidal currents by as much as $\sim$3 km in the course of a cast (Alford et al., 2025). This drift is expected to curtail the extent to which profilers may sample the most vigorous mixing in a tidal cycle, which—as will be seen—takes place immediately below the strongest up-canyon flows. As a profiler descends into these intense flows, it will tend to be advected away from the highly turbulent layers below, potentially introducing a sampling bias. This likely explains why Alford et al. (2025) did not observe buoyancy flux profiles consistent with upwelling.

### 2.3. Calculation of Diapycnal Upwelling From Mooring-Based Temperature Observations

The rate of diapycnal (closely equivalent to diathermal) upwelling, $w_T$*, across the canyon's mean stratification is computed from the mooring-based estimates of $\chi$. An expression for $w_T^*$ may be derived by considering the diathermal flux (Winters & D'Asaro, 1996),

$$\phi = -\kappa \frac{\partial z^*}{\partial T}\left\langle |\nabla T|^2 \right\rangle_{z^*}, \tag{1}$$

where $\kappa$ refers to the molecular diffusivity of seawater, $z$* is the distance in the diathermal direction and $\langle\ \rangle_{z^*}$ denotes an average over a potential temperature surface in a bounded volume. Combining Equation 1 with the definition of $\chi = 2\kappa\left\langle |\nabla T|^2 \right\rangle$ (where the angled brackets indicate an average over a local volume, with spatial scales comparable to those of three-dimensional turbulence; Oakey, 1982) and expressing $w_T^*$ as the rate of change of the diathermal flux in the diathermal direction yields:

$$w_T^* = -\frac{\partial \phi}{\partial z^*} = \frac{1}{2}\frac{\partial\left(\langle\chi\rangle_{z^*}\frac{\partial z^*}{\partial T}\right)}{\partial z^*} = \frac{1}{2}\frac{\partial\langle\chi\rangle_{z^*}}{\partial T} + \frac{1}{2}\langle\chi\rangle_{z^*}\frac{\partial^2 z^*/\partial T^2}{\partial z^*/\partial T}. \tag{2}$$

$w_T^*$ has units of °C s$^{-1}$. Its definition synthesizes the notion that a water parcel mixing with warmer waters more strongly than with colder waters will become warmer, or—since warm waters overlie cold waters in a stably-stratified column—will *upwell* across isotherms. Conversely, a water parcel mixing with colder waters more intensely than with warmer waters will become colder, or *downwell* across isotherms. Note that, since isopycnal gradients of temperature are negligible within the canyon, the in-canyon temperature variance is overwhelmingly produced by diapycnal flows, such that $w_T^*$ is an accurate metric of the diapycnal velocity. $w_T^*$ can be expressed in the more familiar units of m s$^{-1}$ via scaling with the diathermal (close to vertical within the canyon) gradient of potential temperature, that is, $w^* \approx w_T^*/\frac{\partial T}{\partial z^*}$.

Our calculation of $w_T^*$ from mooring-based estimates of $\chi$ makes two inevitable assumptions. First, $z$* is approximated by the local vertical direction, that is, the only direction sampled by the mooring. This approximation is supported by a comparison of directly-measured vertical temperature gradients with indirectlyestimated along-canyon temperature gradients (inferred via application of Taylor's frozen field). This comparison suggests that the characteristic magnitude of vertical gradients typically exceeds that of horizontal gradients by at least one order of magnitude on a wide range of timescales longer than those of the inertial subrange (i.e., $\gg$1 min), such that the diathermal direction is close to vertical on those timescales.

Second, $\langle\chi\rangle_{z^*}$, the isothermal average of $\chi$ within the bounded calculation volume, is assumed to be adequately represented by $\chi$ as sampled by the mooring at a specific tidal phase. Thus, tidal phase-averaged fields of $\chi$ and other relevant variables are constructed prior to computation of $w_T^*$, and the $\langle\ \rangle_{z^*}$ operator is approximated by a tidal phase-average (see Supporting Information S1 for details). There is no a priori justification for this approximation; rather, its adoption places subtle constraints on the interpretation of our $w_T^*$ diagnostics. The "bounded volume" to which these diagnostics apply may be regarded as a body of water centered at the mooring site, extending up to ∼6 km (double the along-canyon semidiurnal tidal excursion) along the thalweg, and sloshing up- and down-canyon by up to ∼3 km. Since the semidiurnal tidal cycle of $\chi$ exhibits the same characteristic patterns at different locations along the canyon (cf. Figure 2c and Figure S3d in Supporting Information S1), our estimated $w_T^*$ at any tidal phase can be thought of as the upwelling rate experienced by the volume at that phase. This would be the case even if different parts of the volume were subject to different tidal phases at any instant in time.

The calculation of $w_T^*$ is performed in four steps. First, a vertical profile of $\chi$ is constructed at 5-min intervals by bin-averaging all the $\chi$ estimates from individual thermistors within a half-bin period of each time-bin center. Second, each vertical profile of $\chi$ is re-mapped onto potential temperature space by bin-averaging in potential temperature cells at intervals of 0.1°C. Third, phase averages of $\chi$ and $z^*$ (approximated by the vertical coordinate) are computed. Fourth, $\partial\chi/\partial T$, $\partial z^*/\partial T$ and $\partial^2 z^*/\partial T^2$ are calculated in each time-bin and potential temperature class via centered differences. This step assumes that a single vertical mooring captures the bulk of the temperature dependence of $\chi$. The resulting estimate of $w_T^*$ is primarily determined by the $\frac{1}{2}\frac{\partial\langle\chi\rangle_{z^*}}{\partial T}$ term, although the contribution from the $\frac{1}{2}\langle\chi\rangle_{z^*}\frac{\partial^2 z^*/\partial T^2}{\partial z^*/\partial T}$ term is also significant and reinforces the patterns in the dominant term (Figure S6 in Supporting Information S1). The uncertainty in $w_T^*$ related to temporal variability and instrumental noise is assessed in the Supporting Information S1, and displayed in Figure 3d.

## 3. Results

A window into the nature of the in-canyon turbulence is provided by the vessel-based timeseries of hydrographic and temperature microstructure profiles, an example of which is shown in Figures 2b and 2c contextualized with the mooring-measured along-canyon flow (Figure 2a). The canyon's background hydrographic structure entails a reduction in potential temperature with depth of ∼1°C over 400 m (Figure 2b), which corresponds to a buoyancy frequency of $\sim 2 \times 10^{-3}$ s$^{-1}$ characteristic of deep-ocean stratification elsewhere (de Lavergne et al., 2016, 2021). This background structure is prominently modulated by a semidiurnal tide, which flows up- and down-canyon with peak speeds of ∼0.2 m s$^{-1}$ (cf. Figures 2a and 2b). As the flood tidal flow displaces isotherms upward, a layer containing frequent patches of unstable stratification (within which temperature typically increases slightly with height above bottom; Figure 2d) develops over 2–3 hr, reaching a height of ∼250 m at the tide's turning. Vigorous mixing ($\chi > 10^{-8}$°C$^2$ s$^{-1}$, exceeding typical ocean-interior values by over one order of magnitude) occurs along the turbulent layer's rising edge (Figure 2c), as isotherms fold over to produce areas of local static instability that progressively mix the fluid from above (Ivey et al., 2021; Thorpe, 2005; Umlauf & Burchard, 2011; van Haren et al., 2024). During the ebb tide, isotherms deepen, the turbulent layer thins rapidly, the near-bottom water column re-stratifies, and elevated mixing is progressively confined closer to the seabed.

Strong shears can induce turbulent mixing of dense and light waters in the stably stratified ocean interior through two primary mechanisms. First, a sufficiently strong and persistent shear can advect dense waters over lighter waters, inducing an overturning instability—sometimes referred to as convective instability (Lorke et al., 2005, 2008; Moum et al., 2004; Umlauf & Burchard, 2011; Winters, 2015). Second, weaker shear can still be energetic enough to trigger a Kelvin-Helmholtz shear instability (Lewin & Caulfield, 2022; Liu et al., 2023; Smyth & Moum, 2012). This is typically assumed to occur when the Richardson number—the ratio of stratification to shear squared—is less than ¼, although for time-dependent shears, as is the case for the tidal flow here, the instability can occur at somewhat higher Richardson numbers (see Supporting Information S1). Both forms of instability,

10.1029/2025GL119186

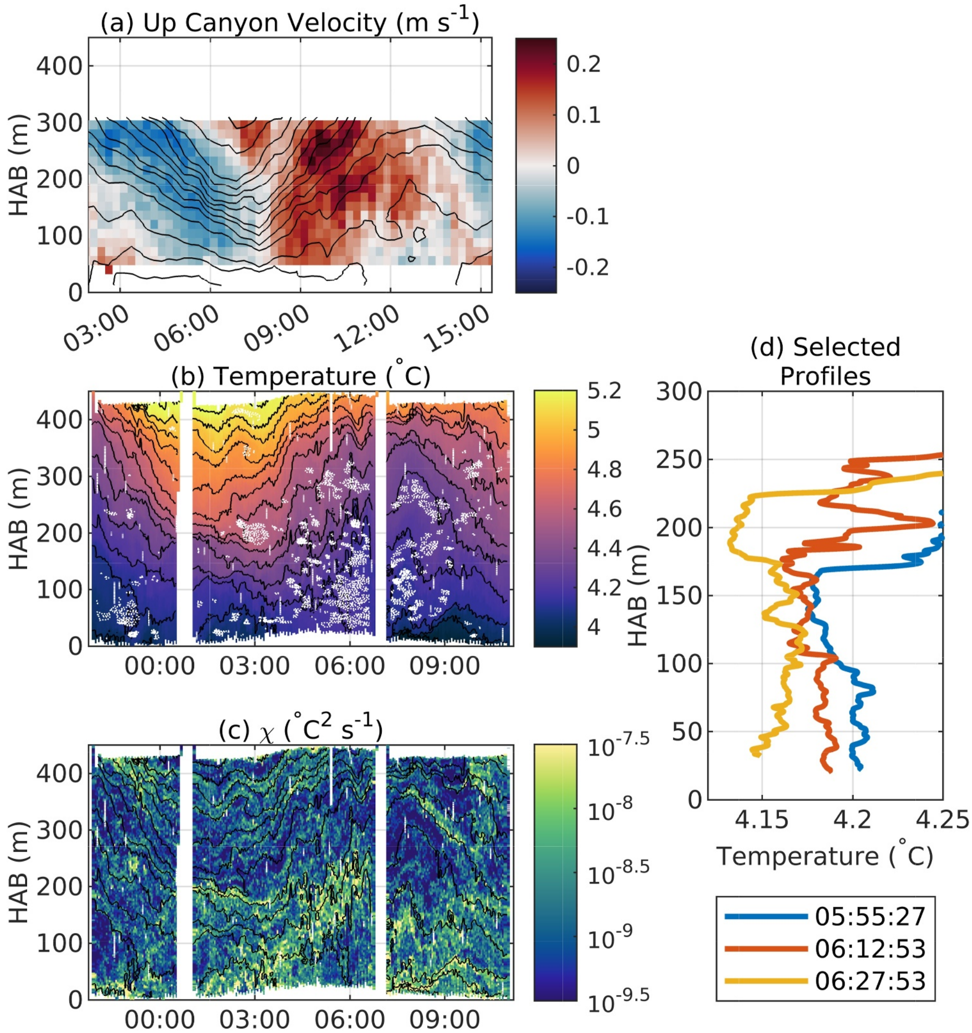


**Figure 2.** A semidiurnal tidal cycle of along-canyon flow, hydrographic structure and turbulent mixing. (a) Along-canyon velocity (shading, positive values indicate up-canyon flow) and potential temperature (contours) measured by the mooring's ADCP and thermistors, respectively, on 8 July 2021. HAB: height above bottom. (b) Potential temperature (shading and black contours) measured by the FastCTD on 2–3 July 2021. White contours indicate occurrences of a statically unstable vertical potential temperature gradient (i.e. $\partial T/\partial z < 0$). (c) Rate of turbulent dissipation of temperature variance ($\chi$, shading) measured by the FastCTD, with potential temperature contours overlaid in black. Panels (a–c), which show data from different periods at approximately the same location, have been aligned by the phase of the semidiurnal tide. (d) Selected profiles of potential temperature during the period with extensive statically unstable conditions.

resulting from either shear-driven overturning or instabilities of a weaker or time-dependent shear, generate patches of elevated turbulence with the same vertical scale of the sheared flow.

The along-canyon tidal flow exhibits significant vertical shear (i.e., the tide is baroclinic; Figure 2a), with flood and ebb tidal speeds usually peaking at >0.15 m s$^{-1}$ about 250 m above the seabed and decreasing to <0.05 m s$^{-1}$ within ~50 m of the bottom. As this vertically-sheared flow advects the background potential temperature distribution—which consists of roughly flat isotherms (Figure 1b)—along the canyon's sloping thalweg, it transports colder waters from further down the canyon over the slowly-moving near-bottom waters during periods of positive shear (upward-increasing up-canyon flow; e.g., during flood), causing unstable stratification and turbulent mixing about 3–6 hr into that tidal phase (Figures 2a and 2b). Conversely, this vertically-sheared flow carries warm waters from higher up the canyon over near-bottom waters during periods of negative shear (downward-increasing up-canyon flow; e.g., during ebb), acting to restore stably-stratified conditions (Figures 2a and 2b). Thus, the occurrence of turbulent mixing and subsequent re-stratification can both be attributed to the

10.1029/2025GL119186

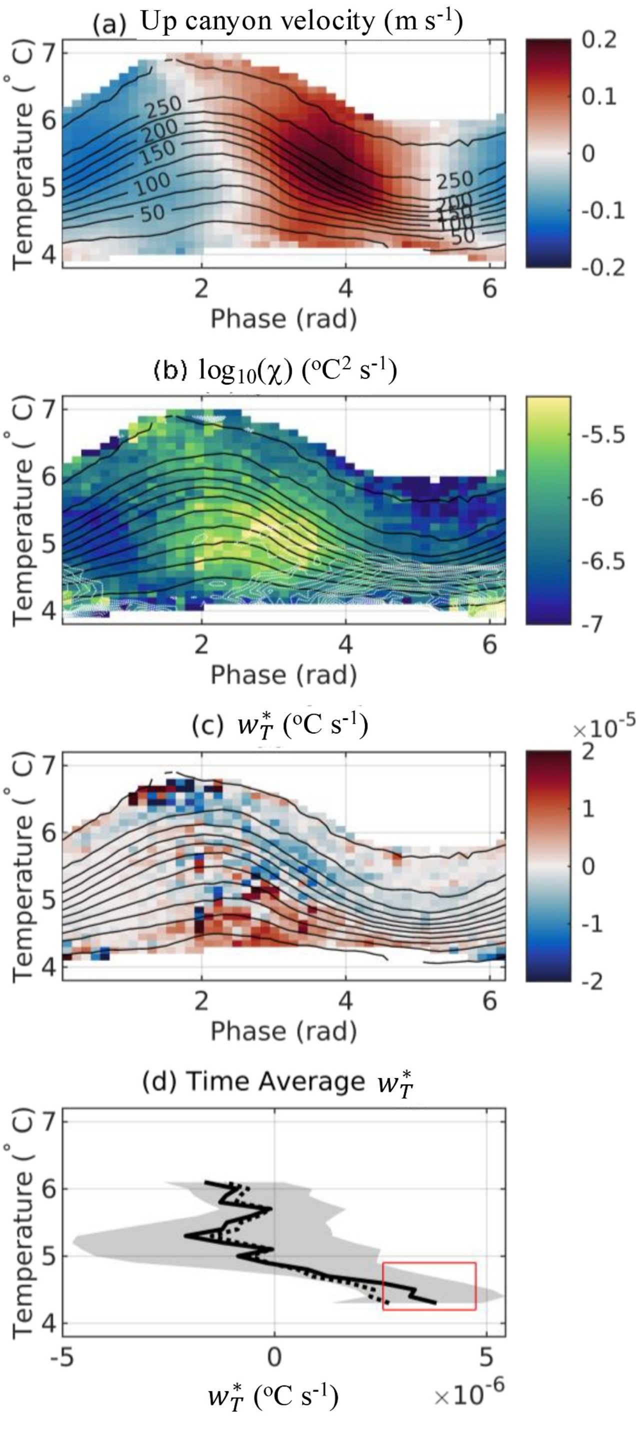


Figure 3.

differential advection of the canyon's background hydrographic structure by a vertically-sheared tide steered by the sloping topography. It remains unclear whether the shear is sufficiently strong and persistent to drive an overturning instability, as argued by Alford et al. (2025), or whether turbulence results from a parametric instability of the time-dependent tidal shear. Both instabilities produce patches of unstable stratification and mixing across the vertical range of enhanced tidal shear, as observed here. See further discussion in the Supporting Information S1.

The role of turbulent mixing in driving the rapid diapycnal upwelling observed in the canyon (Wynne-Cattanach et al., 2024a) may be quantitatively borne out by considering the mooring-based measurements, which—on account of their long extent (89 days) and high temporal resolution (∼1 s)—capture the variability of mixing (assessed via $\chi$; Section 2.2) over many tidal cycles. The same semidiurnal sequence of isotherm shoaling and deepening, de- and re-stratification, and enhancement and suppression of $\chi$, seen in the vessel-based observations (Figure 2) is apparent in the mooring records (Figure S3 in Supporting Information S1, Movie), which also expose some differences between any two tidal cycles. To draw statistically robust relationships between mixing and its tidal drivers, and elucidate implications for upwelling, we construct a phase-averaged picture of the temporal evolution of the along-canyon flow (Figure 3a) and $\chi$ (Figure 3b) over a semidiurnal tidal cycle (see Supporting Information S1). Using $T$ as the vertical coordinate provides a ready connection between $\chi$ and the diathermal (here equivalent to diapycnal) velocity, $w_T$*, expressed as a warming rate and defined by Equation 2.

The phased-averaged view (Figure 3c) demonstrates how, in a characteristic tidal cycle, isobaths progressively converge in potential temperature space (denoting de-stratification; Figure 3a) and $\chi$ is elevated across a wide range of temperatures (Figure 3b) when the flow ∼200 m above the seabed is directed up-canyon relative to the near-bottom flow, that is, precisely when positive shear peaks and stratification is minimal. This occurs at the tide's turning from ebb to flood (around a phase of 2 rad, when the flows far above and near the seabed are oriented oppositely) and during flood (in the phase range of 2.5–5 rad, when flow is up-canyon at all temperatures). The causal relationship between positive shear and $\chi$ also transpires in the latter's diathermal distribution: $\chi$ peaks along the band of maximum up-canyon shear, some ∼120 m above the seabed (Figure 3b; see also Figure S5g in Supporting

**Figure 3.** Phase-averaged semidiurnal tidal cycle of along-canyon flow, turbulent mixing and diapycnal upwelling. Phase-averaged (a) up-canyon velocity, (b) rate of turbulent dissipation of temperature variance ($\chi$), and (c) diapycnal velocity ($w_T^*$)—indicated by shading in each panel—as a function of potential temperature for a characteristic semidiurnal tidal cycle. Height above bottom contours are overlaid in black and labeled in (a). (d) Mean (across all phases) profile of diapycnal velocity as a function of potential temperature. The solid and dashed lines respectively show the diapycnal velocity calculated using dissipation ratio ($\Gamma$) values of 0.2 and 0.4 (see Supporting Information S1). The gray shading provides a measure of the uncertainty in $w_T^*$ related to temporal variability and instrumental noise. This is computed as the interquartile range of $w_T^*$ estimates obtained from many phased-averaged $\chi$ fields, each constructed from a set of three semidiurnal tidal periods. The diapycnal velocity determined from the dye (Wynne-Cattanach et al., 2024a) is added as a rectangle (with horizontal and vertical side lengths respectively indicating the uncertainty and the potential temperature range sampled by the dye, where this range has been shifted toward warmer waters by the difference between the coldest temperatures sampled by the dye and the mooring) for comparison.

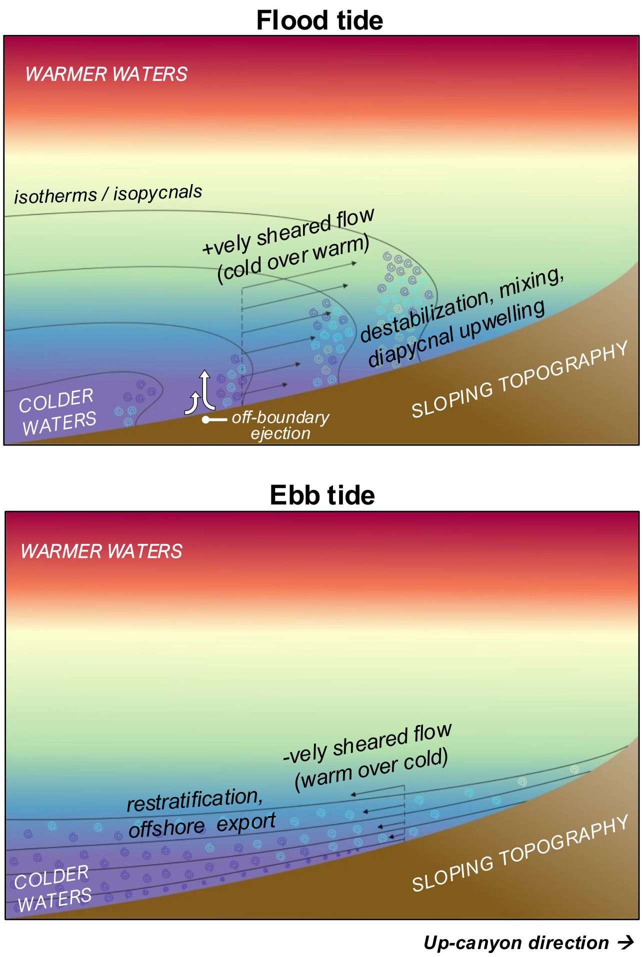


**Figure 4.** Schematic of along-boundary upwelling driven by tidal shear. (a) During flood tide, the positively sheared up-canyon flow (black arrows) causes relatively dense waters aloft to overshoot, reducing stratification and producing mixing with lighter waters via overturning and/or parametric instabilities—thus leading to diapycnal upwelling of the dense waters along the boundary. (b) During ebb tide, the intensification of down-canyon flow with height (negatively sheared flow, shown by black arrows) induces re-stratification within the canyon, and supports the offshore export of waters that were newly mixed and upwelled during the previous flood tide. The small circular swirls in both panels denote turbulent eddies, shaded by temperature/density.

Information S1), and decays toward colder temperatures from there, since the intensity of up-canyon flow varies little over the coldest waters, that is, in the deepest ~80 m. Subsequently, as the tide turns to ebb (in the phase ranges of 0–1.5 rad and >5 rad), isobath divergence and a reduction in $\chi$ lead to re-stratification and suppression of turbulence.

The diapycnal circulation induced by the in-canyon turbulent mixing is illustrated by the phase-averaged distribution of $w_T$* (Figure 3c). During flood, the preferential elevation of $\chi$ within intermediate temperature classes (around 5°C; Figure 3b) results in diapycnal upwelling (i.e., warming) of colder waters (typically within ∼120 m of the seabed) at rates approaching or exceeding $10^{-5}$°C s$^{-1}$, and in somewhat less intense diapycnal downwelling (i.e., cooling) of warmer waters aloft. Little diapycnal flow occurs during ebb. Upon averaging over the tidal cycle to estimate the net diapycnal velocity profile (Figure 3d), waters colder than ~5°C are found to upwell at a rate of up to ~3 × $10^{-6}$°C s$^{-1}$ (~0.3°C d$^{-1}$), and warmer waters to downwell at a weaker rate of ~−1 × $10^{-6}$°C s$^{-1}$ (~−0.1°C d$^{-1}$), resulting in convergence and net formation of waters of intermediate temperatures (around ~5°C). The net upwelling rate of the colder waters approximately matches the dye-derived diapycnal flow of ~0.3°C d$^{-1}$ (Wynne-Cattanach et al., 2024a)—thereby endorsing the role of tidal shear-generated mixing in driving the rapid along-boundary upwelling measured within the canyon.

The efficacy of tidal shear-generated turbulence as an agent of intense diapycnal upwelling is contingent on its large vertical scale, which leads to the swift mixing of waters spanning a substantial range of temperatures. In our measured canyon, where turbulence is observed to reach up to ~250 m above bottom, such vertical scale is determined by that of the along-canyon flow's vertical shear—as it is this shear that reduces stratification by differentially advecting the background temperature profile along the canyon's sloping thalweg (Figure S1 in Supporting Information S1). Our analysis (see Supporting Information S1 and Figure S4 therein) suggests that the in-canyon vertical shear is associated with baroclinic tidal waves that develop within the canyon (Baines, 1983; Grimshaw et al., 1985). The characteristic vertical scale of the waves is on the order of the canyon's vertical extent, which thus sets the size of the large turbulent overturns underpinning along-slope upwelling.

## 4. Conclusions

In conclusion, our observations of a continental-slope canyon at the edge of a North Atlantic basin provide evidence of very rapid along-boundary upwelling driven by vertically extensive turbulent mixing, itself generated by semidiurnal baroclinic tidal flows sloshing up- and down-canyon (Figure 4). The cornerstone of the upwelling mechanism is the sheared structure of the tidal waves that develop within the canyon. When steered by the canyon's sloping thalweg, this shear advects dense waters above lighter near-bottom waters during flood, thereby reducing stratification and priming the BBL for overturning and parametric instabilities. These instabilities produce overturns that mix dense BBL waters with surrounding lighter waters (Figure 4a), resulting in diapycnal upwelling along the canyon. Reversal of the sheared tidal flow during ebb induces re-stratification within the canyon via the differential down-canyon advection of near-boundary waters (Figure 4b), and promotes the offshore export of waters that were newly mixed and upwelled along topography during the previous flood (Wynne-Cattanach et al., 2024a). Such ebb-time re-stratification and export reset the canyon for the next flood stage of upwelling, and communicate the effects of in-canyon mixing and upwelling toward the basin's interior.

Although the technological complexity of our measurements inevitably confines our study to a single small domain, there is evidence to suggest that our findings may have wider representativeness along other sloping boundaries. Such evidence comes in two forms. First, canyons of a similar nature to that of the one targeted here abound around the global continental slope. Our measured canyon's length (∼30 km), width (∼8 km at its mouth), vertical extent (>1,000 m from mouth to head), aspect ratio (∼80°, denoting a relatively narrow canyon), V-shaped geometry (with axial slope near M2 tidal criticality, and steep, supercritical sidewalls), and characteristic barotropic tidal speeds (∼0.08 m $s^{-1}$)—all factors likely to shape the governing physics and intensity of the in-canyon mixing (Nazarian & Legg, 2017a, 2017b)—are in line with those of many continental-slope canyons in the global ocean (P. T. Harris & Whiteway, 2011; Harris et al., 2014; Nazarian et al., 2021). The degree of criticality of the thalweg is likely to be particularly important in generating the strong near-bottom baroclinic flows required to support mixing as vigorous as that in our measured canyon (Sarkar & Scotti, 2017; Slinn & Riley, 1996; Nazarian & Legg, 2017a, 2017b; Nazarian et al., 2021). Second, despite the potential specificity of mixing and upwelling phenomena in canyons (Schubert et al., 2025), observational and modeling investigations of near-boundary mixing in a range of oceanic (Baker et al., 2023; Masunaga et al., 2025; Moum et al., 2004; Schulz & Umlauf, 2016; Umlauf & Burchard, 2011; Winters, 2015), limnic (Lorke et al., 2005, 2008) and idealized geophysical fluid (Lewin & Caulfield, 2022; Liu et al., 2023) settings suggest that the shear-driven destabilization process documented here may be of some generality to oscillatory flows over sloping topography, regardless of the details of the flow or topographic configuration. On this basis, our results provide observational support for the paradigm of BBL-focussed deep-ocean upwelling, and point to shear-generated instabilities as a potentially important agent of such upwelling.

## Conflict of Interest

The authors declare no conflicts of interest relevant to this study.

## Data Availability Statement

The microstructure data are publicly available at Wynne-Cattanach et al. (2024b). The mooring data are publicly available at Voet, Alford, Polzin, Naveira Garabato, Kawamato, et al. (2024). The multi-beam bathymetry data are publicly available at Voet, Alford, Polzin, Naveira Garabato, Wynne-Cattanach, et al. (2024).

**Acknowledgments**

The BLT programme is supported by the U.S. National Science Foundation (Grants OCE-1756264, OCE-1756324) and the U.K. Natural Environment Research Council (Grant NE/S001433/1). We are grateful to the scientific party, crew and technicians on the RRS Discovery for their hard work during data collection; and to Kurt Polzin, Sjoerd Groeskamp and Hans van Haren for their insightful feedback on the manuscript.

## References

Alford, M. H., Wynne-Cattanach, B., Le Boyer, A., Couto, N., Voet, G., Spingys, C. P., et al. (2025). Buoyancy flux and mixing efficiency from direct, near-bottom turbulence measurements in a submarine canyon. *Journal of Physical Oceanography*, *55*(2), 97–118. https://doi.org/10.1175/jpo-d-24-0005-1

Armi, L. (1979a). Some evidence for boundary mixing in the deep ocean. *Journal of Geophysical Research*, *83*(C4), 1971–1979. https://doi.org/10.1029/jc083ic04p01971

Armi, L. (1979b). Reply to comments by C. Garrett. *Journal of Geophysical Research*, *84*(C8), 5097–5098. https://doi.org/10.1029/jc084ic08p05097

Baines, P. G. (1983). Tidal motion in submarine canyons—A laboratory experiment. *Journal of Physical Oceanography*, *13*(2), 310–328. https://doi.org/10.1175/1520-0485(1983)013<0310:tmiscl>2.0.co;2

Baker, L. E., Mashayek, A., & Naveira Garabato, A. C. (2023). Boundary upwelling of Antarctic bottom water by topographic turbulence. *AGU Advances*, *4*(5), e2022av000858. https://doi.org/10.1029/2022av000858

Bluteau, C. E., Jones, N. L., & Ivey, G. N. (2013). Turbulent mixing efficiency at an energetic ocean site. *Journal of Geophysical Research*, *118*(9), 4662–4672. https://doi.org/10.1002/jgrc.20292

de Lavergne, C., Groeskamp, S., Zika, J., & Johnson, H. (2021). The role of mixing in the large-scale ocean circulation. In M. P. Meredith & A. C. Naveira Garabato (Eds.), *Ocean Mixing: Drivers, Mechanisms and Impacts*. Elsevier.

de Lavergne, C., Madec, G., Le Sommer, J., Nurser, A. J. G., & Naveira Garabato, A. C. (2016). On the consumption of Antarctic bottom water in the abyssal ocean. *Journal of Physical Oceanography*, *46*(2), 635–661. https://doi.org/10.1175/jpo-d-14-0201.1

Drake, H. F., Ferrari, R., & Callies, J. (2020). Abyssal circulation driven by near-boundary mixing: Water mass transformations and interior stratification. *Journal of Physical Oceanography*, *50*(8), 2203–2226. https://doi.org/10.1175/jpo-d-19-0313.1

Ferrari, R., Mashayek, A., McDougall, T. J., Nikurashin, M., & Campin, J.-M. (2016). Turning ocean mixing upside down. *Journal of Physical Oceanography*, *46*(7), 2239–2261. https://doi.org/10.1175/jpo-d-15-0244.1

Garrett, C. (1979). Comment on "some evidence for boundary mixing in the deep ocean" by L. Armi. *Journal of Geophysical Research*, *84*(C8), 5095. https://doi.org/10.1029/jc084ic08p05095

Garrett, C. (1990). The role of secondary circulation in boundary mixing. *Journal of Geophysical Research*, *95*(C3), 3181–3188. https://doi.org/10.1029/jc095ic03p03181

Gregg, M. C., D'Asaro, E. A., Riley, J. J., & Kunze, E. (2018). Mixing efficiency in the ocean. *Annual Review of Marine Science*, *10*(1), 443–473. https://doi.org/10.1146/annurev-marine-121916-063643

Grimshaw, R. H. J., Baines, P. G., & Bell, R. C. (1985). The reflection and diffraction of internal waves from the junction of a slit and a half-space, with application to submarine canyons. *Dynamics of Atmospheres and Oceans*, *9*(2), 85–120. https://doi.org/10.1016/0377-0265(85)90001-6

Harris, P., Macmillan-Lawler, M., Rupp, J., & Baker, E. (2014). Geomorphology of the oceans. *Marine Geology*, *352*, 4–24. https://doi.org/10.1016/j.margeo.2014.01.011

Harris, P. T., & Whiteway, T. (2011). Global distribution of large submarine canyons: Geomorphic differences between active and passive continental margins. *Marine Geology*, *285*(1–4), 69–86. https://doi.org/10.1016/j.margeo.2011.05.008

Holliday, N. P., Cunningham, S. A., Johnson, C., Gary, S. F., Griffiths, C., Read, J. F., & Sherwin, T. (2015). Multidecadal variability of potential temperature, salinity, and transport in the eastern subpolar North Atlantic. *Journal of Geophysical Research*, *120*(9), 5945–5967. https://doi.org/10.1002/2015jc010762

Ivey, G. N., Bluteau, C. E., Gayen, B., Jones, N. L., & Sohail, T. (2021). Roles of shear and convection in driving mixing in the ocean. *Geophysical Research Letters*, *48*(3), e2020gl089455. https://doi.org/10.1029/2020gl089455

Klymak, J. M., Pinkel, R., Liu, C.-T., Liu, A. K., & David, L. (2006). Prototypical solitons in the South China Sea. *Geophysical Research Letters*, *33*(11), L11607. https://doi.org/10.1029/2006gl025932

Kunze, E. (2017a). Internal-wave-driven mixing: Global geography and budgets. *Journal of Physical Oceanography*, *47*(6), 1325–1345. https://doi.org/10.1175/jpo-d-16-0141.1

Kunze, E. (2017b). The internal-wave-driven meridional overturning circulation. *Journal of Physical Oceanography*, *47*(11), 2673–2689. https://doi.org/10.1175/jpo-d-16-0142.1

Lewin, S. F., & Caulfield, C. P. (2022). Stratified turbulent mixing in oscillating shear flows. *Journal of Fluid Mechanics*, *944*, R3. https://doi.org/10.1017/jfm.2022.537

Liu, C.-L., Kaminski, A. K., & Smyth, W. D. (2023). The effects of boundary proximity on Kelvin-Helmholtz instability and turbulence. *Journal of Fluid Mechanics*, *966*, A2. https://doi.org/10.1017/jfm.2023.412

Lorke, A., Peeters, F., & Wüest, A. (2005). Shear-induced convective mixing in bottom boundary layers on slopes. *Limnology & Oceanography*, *50*, 1612–1619.

Lorke, A., Umlauf, L., & Mohrholz, V. (2008). Stratification and mixing on sloping boundaries. *Geophysical Research Letters*, *35*(14), L14610. https://doi.org/10.1029/2008gl034607

Lumpkin, R., & Speer, K. (2007). Global ocean meridional overturning. *Journal of Physical Oceanography*, *37*(10), 2550–2562. https://doi.org/10.1175/jpo3130.1

MacKinnon, J., Zhao, Z., Whalen, C. B., Waterhouse, A. F., Trossman, D. S., Sun, O. M., et al. (2017). Climate process team on internal wave-driven ocean mixing. *Bulletin of the American Meteorological Society*, *98*(11), 2429–2454. https://doi.org/10.1175/bams-d-16-0030.1

Masunaga, E., Alford, M. H., & Bellerjeau, C. (2025). Mechanisms of internal tide-induced turbulent mixing observed from mooring data in a shallow steep submarine canyon. *Journal of Physical Oceanography*, *55*(9), 1607–1622. https://doi.org/10.1175/jpo-d-24-0132.1

Melet, A., Hallberg, R., & Marshall, D. P. (2021). The role of ocean mixing in the climate system. In M. P. Meredith & A. C. Naveira Garabato (Eds.), *Ocean Mixing: Drivers, Mechanisms and Impacts*. Elsevier.

Moum, J., Perlin, A., Klymak, J. M., Levine, M. D., Boyd, T., & Kosro, P. M. (2004). Convectively driven mixing in the bottom boundary layer. *Journal of Physical Oceanography*, *34*(10), 2189–2202. https://doi.org/10.1175/1520-0485(2004)034<2189:cdmitb>2.0.co;2

Munk, W. (1966). Abyssal recipes. *Deep-Sea Research*, *13*(4), 707–730. https://doi.org/10.1016/0011-7471(66)90602-4

Munk, W., & Wunsch, C. (1998). Abyssal recipes II: Energetics of tidal and wind mixing. *Deep-Sea Research I*, *45*(12), 1977–2010. https://doi.org/10.1016/s0967-0637(98)00070-3

Nazarian, R. H., Burns, C. M., Legg, S., Buijsman, M. C., Kaur, H., & Arbic, B. K. (2021). On the magnitude of canyon-induced mixing. *Journal of Geophysical Research*, *126*(11), e2021jc017671. https://doi.org/10.1029/2021jc017671

Nazarian, R. H., & Legg, S. (2017a). Internal wave scattering in Continental slope canyons, part 1: Theory and development of a ray tracing algorithm. *Ocean Modelling*, *118*, 1–15. https://doi.org/10.1016/j.ocemod.2017.07.002

Nazarian, R. H., & Legg, S. (2017b). Internal wave scattering in Continental slope canyons, part 2: A comparison of ray tracing and numerical simulations. *Ocean Modelling*, *118*, 16–30. https://doi.org/10.1016/j.ocemod.2017.07.005

Oakey, N. S. (1982). Determination of the rate of dissipation of turbulent energy from simultaneous temperature and velocity shear microstructure measurements. *Journal of Physical Oceanography*, *12*(3), 256–271. https://doi.org/10.1175/1520-0485(1982)012<0256:dotrod>2.0.co;2

Polzin, K. L., & McDougall, T. J. (2021). Mixing at the ocean's bottom boundary. In M. P. Meredith & A. C. Naveira Garabato (Eds.), *Ocean Mixing: Drivers, Mechanisms and Impacts*. Elsevier.

Sarkar, S., & Scotti, A. (2017). From topographic internal gravity waves to turbulence. *Annual Review of Fluid Mechanics*, *49*(1), 195–220. https://doi.org/10.1146/annurev-fluid-010816-060013

Schubert, R., Gula, J., Capó, E., Damien, P., Molemaker, M. J., Vic, C., & McWilliams, J. (2025). The ocean flows downhill near the seafloor and recirculates upward above. *Nature Communications*, *16*(1), 5873. https://doi.org/10.1038/s41467-025-61027-2

Schulz, K., & Umlauf, L. (2016). Residual transport of suspended material by tidal straining near sloping topography. *Journal of Physical Oceanography*, *46*(7), 2083–2102. https://doi.org/10.1175/jpo-d-15-0218.1

Shaw, W. J., Trowbridge, J. H., & Williams, A. J., III. (2001). Budgets of turbulent kinetic energy and scalar variance in the Continental shelf bottom boundary layer. *Journal of Geophysical Research*, *106*(C5), 9551–9564. https://doi.org/10.1029/2000jc000240

Slinn, D. N., & Riley, J. J. (1996). Turbulent mixing in the Oceanic boundary layer caused by internal wave reflection from sloping terrain. *Dynamics of Atmospheres and Oceans*, *24*(1–4), 51–62. https://doi.org/10.1016/0377-0265(95)00425-4

Smyth, W. D., & Moum, J. N. (2012). Ocean mixing by Kelvin-Helmholtz instability. *Oceanography*, *25*(2), 140–149. https://doi.org/10.5670/oceanog.2012.49

Sreenivasan, K. R. (2018). Turbulent mixing: A perspective. *Proceedings of the National Academy of Sciences*, *116*(37), 18175–18183. https://doi.org/10.1073/pnas.1800463115

Stanev, E. V., & Ricker, M. (2020). Interactions between barotropic tides and mesoscale processes in deep ocean and shelf regions. *Ocean Dynamics*, *70*(5), 713–728. https://doi.org/10.1007/s10236-020-01348-6

Talley, L. D. (2013). Closure of the global overturning circulation through the Indian, Pacific, and Southern Oceans: Schematics and transports. *Oceanography*, *26*(1), 80–97. https://doi.org/10.5670/oceanog.2013.07

Thorpe, S. A. (2005). *The turbulent ocean*. Cambridge University Press.

Umlauf, L., & Burchard, H. (2011). Diapycnal transport and mixing efficiency in stratified boundary layers near sloping topography. *Journal of Physical Oceanography*, *41*(2), 329–345. https://doi.org/10.1175/2010jpo4438.1

van Haren, H., Voet, G., Alford, M. H., Fernández-Castro, B., Naveira Garabato, A. C., Wynne-Cattanach, B. L., et al. (2024). Near-slope turbulence in a Rockall canyon. *Deep-Sea Research I*, *206*, 104277. https://doi.org/10.1016/j.dsr.2024.104277

Voet, G., Alford, M., Polzin, K., Naveira Garabato, A., Kawamato, S., Dufel, H., et al. (2024). Boundary layer turbulence and abyssal recipes (BLT): Moored observations [Dataset]. *Dryad*. https://doi.org/10.5061/dryad.v15dv424f

Voet, G., Alford, M., Polzin, K., Naveira Garabato, A., Wynne-Cattanach, B., Couto, N., et al. (2024). Boundary layer turbulence and abyssal recipes (BLT): Multibeam bathymetry dataset [Dataset]. *SEANOE*. Retrieved from https://www.seanoe.org/data/00887/99872

Waterhouse, A. F., MacKinnon, J. A., Nash, J. D., Alford, M. H., Kunze, E., Simmons, H. L., et al. (2014). Global patterns of diapycnal mixing from measurements of the turbulent dissipation rate. *Journal of Physical Oceanography*, *44*(7), 1854–1872. https://doi.org/10.1175/jpo-d-13-0104.1

Whalen, C. B., de Lavergne, C., Naveira Garabato, A. C., Klymak, J. M., MacKinnon, J. A., & Sheen, K. L. (2020). Internal wave-driven mixing: Governing processes and consequences for climate. *Nature Reviews Earth & Environment*, *1*(11), 606–621. https://doi.org/10.1038/s43017-020-0097-z

Winters, K. B. (2015). Tidally driven mixing and dissipation in the stratified boundary layer above steep submarine topography. *Geophysical Research Letters*, *42*(17), 7123–7130. https://doi.org/10.1002/2015gl064676

Winters, K. B., & D'Asaro, E. A. (1996). Diascalar flux and the rate of fluid mixing. *Journal of Fluid Mechanics*, *317*, 179–193. https://doi.org/10.1017/s0022112096000717

Wynne-Cattanach, B., Couto, N., Drake, H. F., Ferrari, R., Le Boyer, A., Mercier, H., et al. (2024a). Observations of diapycnal upwelling within a sloping submarine canyon. *Nature*, *630*(8018), 884–890. https://doi.org/10.1038/s41586-024-07411-2

Wynne-Cattanach, B., Couto, N., Drake, H. F., Ferrari, R., Le Boyer, A., Mercier, H., et al. (2024b). Boundary layer turbulence and abyssal recipes (BLT): Micorostructure and dye survey datasets [Dataset]. *SEANOE*. Retrieved from https://www.seanoe.org/data/00870/98178